Structural Engineering and Mechanics, Vol. 15, No. 5 (2003) 495-511
DOI: http://dx.doi.org/10.12989/sem.2003.15.5.495

Enhancement of the buckling strength of glass beams by means of lateral restraints

J. Belis†, R. Van Impe‡, G. Lagae‡ and W. Vanlaere‡†

Laboratory for Research on Structural Models, Department of Structural Engineering, Ghent University, Technologiepark-Zwijnaarde 904, B-9052 Gent-Zwijnaarde, Belgium

(Received November 13, 2002, Accepted March 11, 2003)

Abstract. New material applications and transparency are desired by contemporary architects. Its superb transparency and high strength make glass a very suitable building material -in spite of its brittleness- even for primary load bearing structures. Currently we will focus on load bearing glass beams, subjected to different loading types. Since glass beams have a very slender, rectangular cross section, they are sensitive to lateral torsional buckling. Glass beams fail under a critical buckling load at stresses that lie far below the theoretical simple bending strength, due to the complex combination of torsion and out-of-plane bending, which characterises the instability phenomenon. The critical load can be increased considerably by preventing the upper rim from moving out of the beam's plane. Different boundary conditions are examined for different loading types. The load carrying capacity of glass beams can be increased three times and more using relatively simple, cheap lateral restraints.

Key words: glass beams; buckling strength; load bearing capacity; lateral torsional buckling; lateral restraints.

1. Introduction

On the one hand, newly developed materials with special material characteristics can put the architect's and engineer's building tools in a new perspective. On the other hand, architectural and engineering dreams can be the trigger to start research in the materials science field -to develop materials with special characteristics on demand- or in the structural engineering field, when new applications of existing materials are aimed at.

Transparency certainly is one of such material characteristics with a high desirability factor in contemporary building designs. The idea itself is not new, and we all know historical examples like e.g., "Crystal Palace", built (and demolished) in London, United Kingdom (Fig. 1) or "The Glass House" in New Canaan, Connecticut (Fig. 2). However, the dream continues nowadays in making also the load bearing structure itself transparent. Glass is a very well suited material to fit those needs. Several realised examples of glass beams and glass columns in Europe illustrate the possibilities and special spatial perception of transparent load carrying structures (Fig. 3).

† Doctoral Assistant
‡ Professor
‡† Scientific co-worker

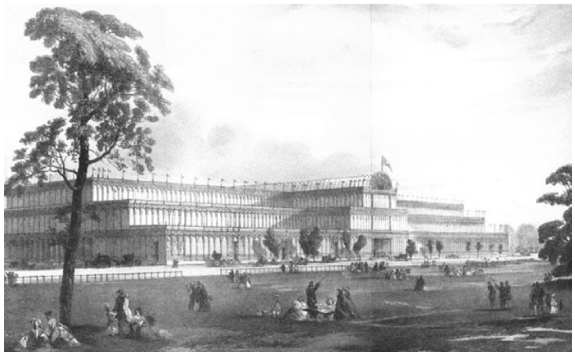

Fig. 1 Crystal Palace by Joseph Paxton, London, 1851

Fig. 2 The Glass House by Philip Johnson, New Cannan, Connecticut, 1949

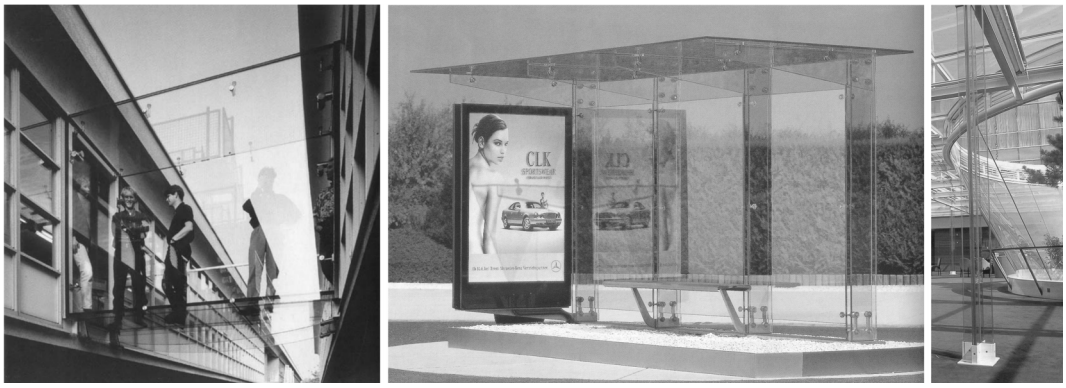

Fig. 3 Examples in Europe: Pedestrian Bridge, Bus Shelter, Roof supporting Column

Nonetheless, developing a load bearing glass construction is not evident. The lack of national or international codes or standards makes it difficult for designers to bring forth economic load bearing glass designs. Official technical control agencies often require expensive full-scale destructive tests that are performed at independent laboratories. Furthermore, designers tend to use exaggerated safety factors, which result from a general lack of experience and reliable scientific structural information. The present uneconomic material use and corresponding high expenses are self-explanatory.

It is clear that several years of further scientific research will be needed for optimisation of load carrying capacity, material use, safety and construction methods. The Laboratory for Research on Structural Models of the Ghent University in Belgium is active in research on the structural behaviour of load bearing glass building components, with the long term objective to help the development of structural load carrying glass design codes (Belis 2000).

2. Material's background

Glass is an interesting structural engineering material. There are hundreds of kinds of glasses,

depending on the chemical constitution. For building purposes, the use of basic soda lime silicate glass is widely spread. Excellent surface flatness and optical qualities for this type of glass are realised by letting the glass melt float on tin under controlled temperature conditions. This industrial technique is well known and called the "float process".

When the strength of glass is considered, one has to distinguish the microscopic scale -where glass strength depends above all on the quality of the molecular bonding and is of the order of magnitude of 3600 to 5000 MPa (ISE 1999)- from the macro scale. In literature one finds characteristic tensile strengths of float glass on a macroscopic scale -i.e., the scale of structural building components- between 10 and 100 MPa. Laboratory experiments showed that values for the tensile strength of chemically prestressed panes could go up to 200 MPa and beyond (Roelandt 2000). In comparison to the microscopic level, the strength levels are greatly reduced due to unavoidable surface imperfections and invisible or nearly visible micro-cracks, caused by the production process, transport and handling. In literature these imperfections are known as Griffith flaws (Griffith 1921, Carré 1997).

Griffith flaws are randomly distributed across the surface of a piece of glass. The probability that a crack will propagate and glass will break equals the probability that a flaw or crack is situated at a critical tensile stress location. The statistical distribution, which is mostly used to express this probability, has been developed by Weibull (Weibull 1951), although the relevance of this theory has been questioned (Calderdone 2001).

By reasons of completeness, we mention the existence of HF-chemical treatments that can chemically remove the outer surfaces and flaws of a glass pane, resulting in strength levels that are closer to the theoretical micro scale strength than glass panes without such a treatment. Special precautions need to be taken in order to preserve the undamaged glass surface state and its according strength.

The combination of a very good transparency with a high strength makes glass a unique building material. The main disadvantage, however, is its total lack of tensile ductility: glass is a brittle material.

In order to assure a certain residual strength, glass beams will usually be conceptually designed as laminates: a number of individual glass panes held together by means of a soft transparent interlayer. Polyvinyl butyral (PVB) or resin are chosen in most cases. In case of a single glass pane failure, pieces stay adhered to the interlayer, and people below are saved from injuries. A residual load carrying capacity results from the unbroken panes and interlayers.

Even with composed glass beams, the geometry of the structural elements is limited to a slender quasi-rectangular cross section. The reason is that there are no connection systems that are suitable to deal with the shear forces between a glass web and flanges. Glues are too much deformable or simply not strong enough, while glass welding induces complicated and structurally unfavourable residual stresses. The technique of glass welding is not very well known.

In this contribution, we focus on the structural behaviour of single-pane glass beams.

3. Load bearing capacity

3.1 Model

The beam model we start our analysis with consists of a single float glass pane with dimensions

Fig. 4 Beam model used in the laboratory

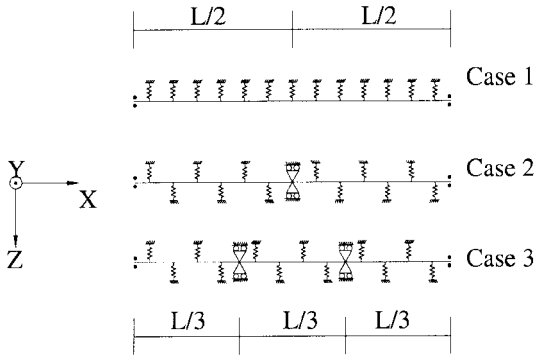

Fig. 5 Boundary condition cases

L = 2200 mm, H = 400 mm and t = 10 mm. This geometry corresponds to the real single pane glass beams, which have been (and will be) used in the Laboratory for Research on Structural Models of the Ghent University (Roelandt 2000). The beam is supported by two fork bearings, which exclude a rotation around the longitudinal axis and lateral movements at the supports (Fig. 4).

3.2 Buckling

Since the considered beams have a very slender cross-section, they are sensitive to lateral torsional buckling. Several authors have proposed expressions to determine the critical load for lateral torsional buckling (EC3 1992, Trahair 1993, …). A comparative study has demonstrated that the results of the different expressions show good agreement (Roelandt 2000, Pattheeuws 2001). For that reason, it is sufficient for our purpose to focus on only one solution, e.g., the one of Eurocode 3 (EC3 1993). The critical moment for lateral torsional buckling M_{cr} is given by:

$$M_{cr} = C_1 \frac{\pi^2 E I_z}{L^2}\left[\left(\frac{I_w}{I_z} + \frac{L^2 G I_t}{\pi^2 E I_z} + (C_2 z_g)^2\right)^{0.5} - C_2 z_g\right] \quad (1)$$

In this expression I_t is the torsion constant, I_w is the warping constant, I_z is the second moment of area about the minor axis, L = 2200 mm is the length of the beam between points which have lateral restraints and z_g = 200 mm is the distance between the point of load application and the shear centre. Values of C_1 and C_2 are given in Eurocode 3 for various load cases. For a point load P at mid span and for a uniform load p on the total length of the beam, values are respectively C_1 = 1.365 or 1.132 and C_2 = 0.553 or 0.459. The obtained critical load P_{cr} is 9319.29 N for a point load at mid span and p_{cr} = 8.47 N/mm for a uniformly distributed load. (This corresponds with a total value of the constant load in the given geometry of 18638.57 N).

3.3 In-plane bending

From classic beam theory we can easily calculate the bending stresses at the outer fibres of the rectangular beam section for the critical loads as obtained above:

$$\sigma = \frac{M}{W} = 20.12 \text{ MPa} \quad \text{for the point load, with } M = \frac{P_{cr}L}{4} \tag{2}$$

$$\sigma = 17.07 \text{ MPa} \quad \text{for the uniform load, with } M = \frac{p_{cr}L^2}{8} \tag{3}$$

W is the section modulus of the rectangular section for bending about the major axis. The maximum appearing stresses due to simple bending are very low when the beam is loaded with the critical load for lateral torsional buckling. On the other hand, if we suppose a typical characteristic tensile strength of 60 MPa for the glass (ISE 1999), loads could go up to 29060.91 MPa for a point load at mid span and 58181.82 MPa for a uniformly distributed load. Characteristic strengths can easily go up to 150 MPa (Roelandt 2000), resulting in even remarkably higher allowable loads if only bending is considered.

The example above shows clearly that the load bearing capacity of glass beams can be improved considerably (critical loads get up to five times as high) if lateral torsional buckling can be excluded and the beam is forced to fail in simple bending. Lateral torsional buckling can be excluded if the compressed rim can be restrained laterally (Hess 2000). The effect of a different partial out-of-plane movement prevention method is examined below.

4. Numerical analysis

4.1 General

At present our study consists of a numerical and experimental analysis. Computer calculations are performed by the finite elements method based computer program Rasta, which has been developed at the Laboratory for Research on Structural Models (Van Impe 1998). The numerical model is made up with a sufficiently dense mesh of Lagrangian shell elements with 9 nodes (Fig. 6). The geometry is identical to the experimental model as described in section 3.1.

Two main loading types are considered. The first is a uniform load over the full length of the beam with a value p = 60 N/mm. The second is a concentrated load at mid span which represents the same total loading force: $P = 60 * 2200 = 132000$ N. Since prevention of lateral movement in a

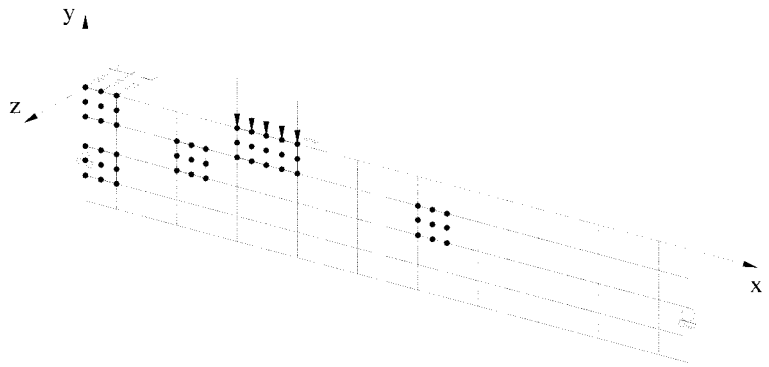

Fig. 6 Numerical model

real construction can vary from zero (i.e. without restraints) to infinity (i.e. laterally totally clasped) -but usually lies somewhere in between-, we introduced lateral springs to support the compressed rim of the beam model.

Springs are attached to the uppermost compressed rim along the whole beam length in all simulations. The influence of the spring stiffness k on the load bearing capacity of the beam is examined numerically by varying its value during the simulations.

4.2 Load factor

We define the load factor λ as the factor by which the basic loads (as determined in the previous paragraph) must be multiplied to determine the total load on the beam. The loads are supposed to keep their verticality during the analysis.

4.3 Uniform load p = 60 N/mm

Three main cases with different boundary conditions are used, as illustrated in Fig. 5.

Case 1 represents the beam, supported by a fork bearing at each end and by continuous lateral springs along the compressed rim. It represents for example a fork supported glass beam, which has its compressed upper rim silicon glued to a glass roof plate. The roof structure itself is supposed to be very stiff in its plane and flexible in the direction perpendicular to its plane.

Case 2 has a supplementary restraint, which doesn't allow any out-of-plane movement of the compressed rim: it has only its Z-direction fixed at mid span. This model simulates the influence of e.g. a stabilising cable with a high longitudinal stiffness at both sides of the beam.

Case 3 has two such restraints, with a spacing of a third of the total span.

4.3.1 Observations

In general it is noticed that higher spring stiffnesses result in an important increase of the load factors. The use of lateral "spring" supports can seriously augment the lateral torsional buckling resistance of the beams in all cases. The results of the analysis are compiled in Fig. 7.

For a beam without any lateral spring supports (k = 0 kN/cm) the load factor increases quickly when an increasing number of lateral restraints is added. This corresponds with buckling loads p_{cr1} = 7.2, p_{cr2} = 18.0 and p_{cr3} = 24.0 N/mm for the first, second and third case respectively. For beams without lateral springs, the addition of point-wise lateral restraints has a positive effect on their load bearing capacity, as could be expected.

Higher values of the spring stiffness (k > 0 kN/cm) result in a considerable growth of the load factor, especially for beams without additional lateral restraints (case 1). The graph of case 1 shows a very steep part for 0 < k < 0.2 kN/cm, indicating that an important improvement of the load carrying capacity can be achieved even with relatively weak springs on a beam that is supported by two fork bearings. The same effect is noticed for beams with one lateral restraint, but in a less spectacular way. The steeper part of the curve is situated in the region 0 < k < 0.3 kN/cm. For a beam with two or more lateral restraints, the curve is approximately linear and no steep part exists.

The lines of case 1 and case 3 intersect and are virtually identical in the interval 0 < k < 0.4 kN/cm. For k > 0.4 kN/cm the difference between both cases is not very important either. It seems that the addition of two lateral restraints as in case 3 has a poor effect for values of the spring stiffness, which exceed 0.1 kN/cm. The addition of only one restraint at mid span, on the contrary, has a

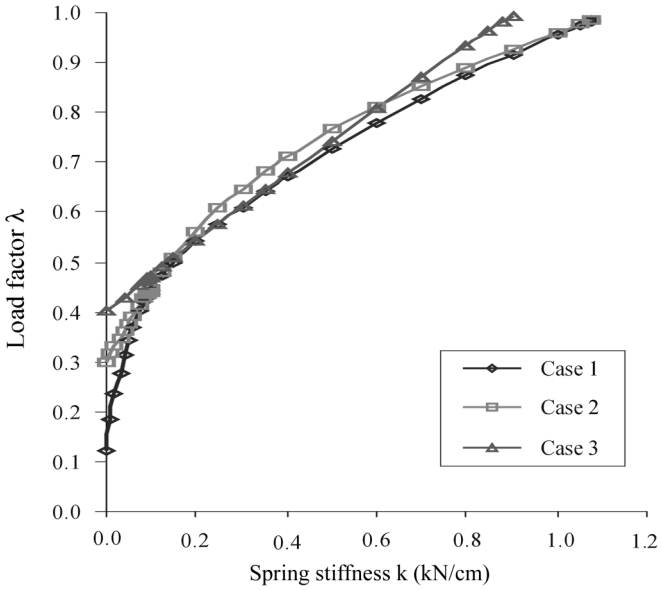

Fig. 7 Results for the uniform load

positive effect on the load bearing capacity, except for values of k in the neighbourhood of 0.15 kN/cm and above 1.0 kN/cm, where the other curves are intersected.

Only the lower values of the spring stiffness are displayed in the graphs, because all curves will have the same asymptotic value for infinitely high values of the spring stiffness. It is obvious that in that case all fixed individual lateral restraints are redundant and of no influence anymore.

4.3.2 Buckling modes

When the lateral torsional buckling load is reached, the cross-sections of the beam will rotate and move out of the *xy*-plane all of a sudden. We are aware of the fact that our bifurcation analyses do not make it possible to calculate exact lateral torsional displacements and the eigenmodes found are not more than a means of visualising what will happen in the very critical stage of buckling.

From the numerical analysis, it is possible to visualise the buckling modes for different boundary condition cases.

If no lateral springs are present (k = 0 kN/cm), the second eigenmode for an unrestrained beam becomes the first eigenmode for a beam with one lateral support at mid span (Fig. 8, upper left). In analogy, the third eigenmode for an unrestrained beam becomes visible if two fixed lateral supports are positioned at one third of the span (Fig. 8, upper right).

It can be seen that the basic deformation shape of a buckling beam with boundary condition case 3 undergoes virtually no changes when the stiffness of the elastic sideward supports is adjusted (Fig. 8, right column from top to bottom). The corresponding load factors vary linearly with the spring stiffness k.

On the other hand, important changes in the buckling mode appear when a beam with boundary condition case 2 is confronted with gradually increasing spring stiffnesses of the continuous elastic supports. In the left column (Fig. 8), it can be noticed that the original shape for k = 0 kN/cm,

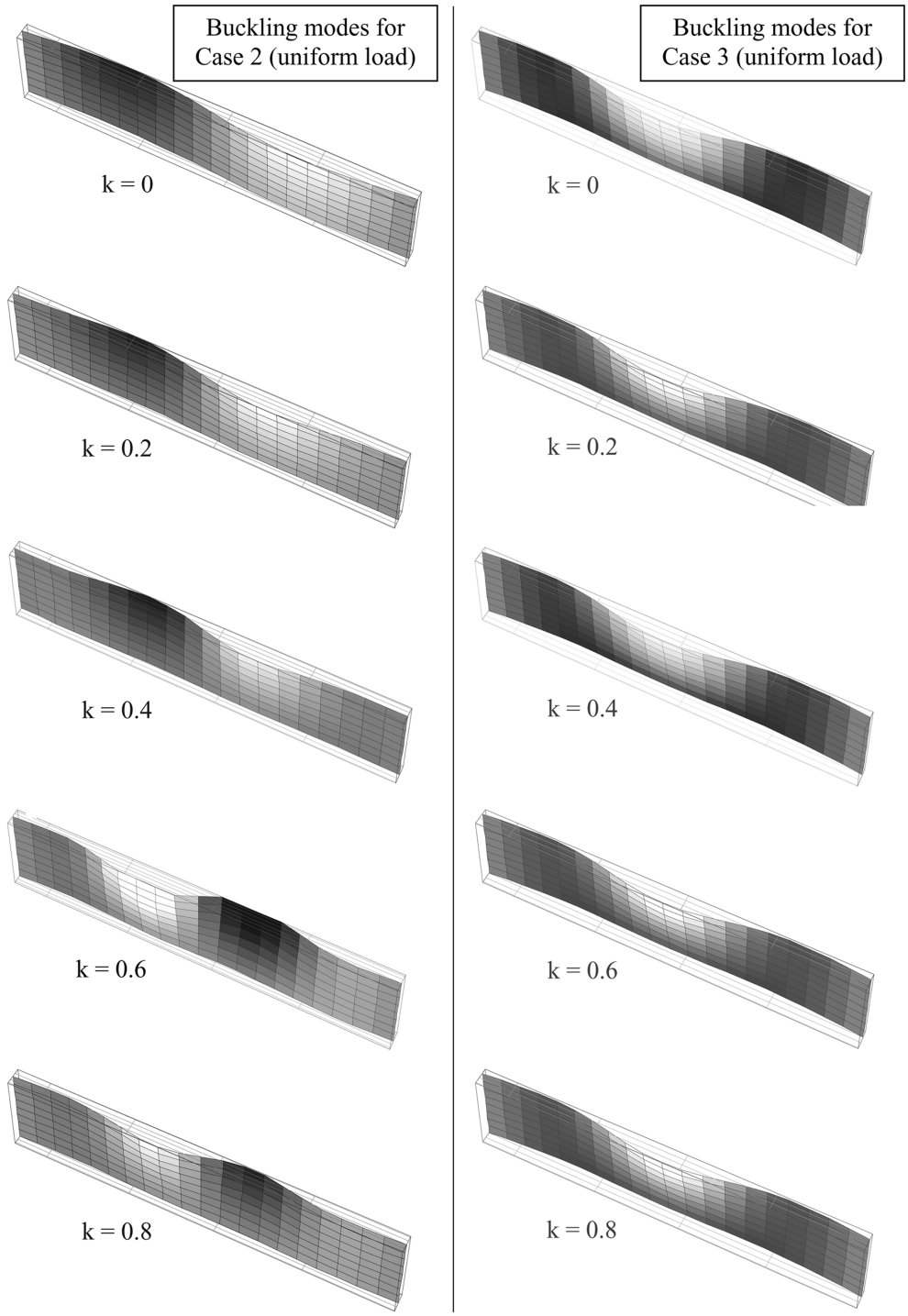

Fig. 8 Comparison of buckling modes under a uniform load, for an increasing spring stiffness k [kN/cm], and for boundary condition cases 2 and 3

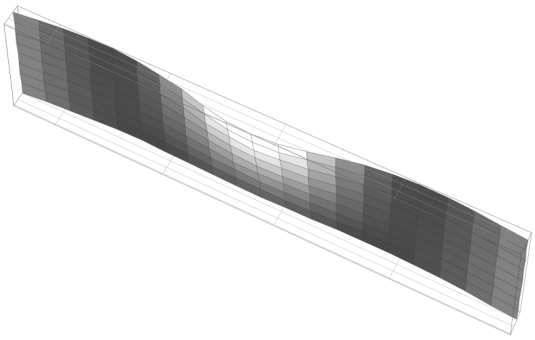

Fig. 9 Buckling mode for case 1, k = 0.4 kN/cm

which has only one point of inflection, changes towards a configuration with three points of inflection. Throughout the process, both beam-ends seem to be gradually tightened towards the straight centre line of the undeformed glass pane. The wavelength of the sinusoidal waves decreases accordingly.

For values of k between approximately 0.2 and 0.6 kN/cm, the eigenmodes of case 2 differ from those of case 3. The effect on the critical buckling load is demonstrated clearly by the intersecting curves in Fig. 7. Fig. 7 reveals the surprising effect that the addition of more fixed lateral supports (case 3) does not necessarily result in a bigger increase of load carrying capacity. The reason is that the buckling modes for case 2, for the values of k approximately between 0.2 and 0.6 kN/cm, correspond with higher eigenvalues for the load factor than the buckling modes of case 3. When the buckling modes for e.g. k = 0.4 kN/cm are compared, it is seen that the general deformation of the upper rim consists roughly of three half sinusoidal waves for case 1 (Fig. 9) and case 3 (right column of Fig. 8), where four half waves -clearly a higher eigenmode- are counted for case 2 (left column of Fig. 8). For values of k higher than 0.6 kN/cm, the eigenmode of case 2 is lower than the other cases because of the increasing clamping effect of the springs, especially near the supports.

4.4 Point load P = 132000 N

For the point-wise loading type, only boundary condition cases 1 and 2 are examined (Fig. 5). In analogy with the previous loading type, a meaningful difference is noticed in the initial load factors of case 1 and case 2 (k = 0 kN/cm). Here too, an additional lateral support increases the load bearing capacity of the beam considerably: the addition of one lateral support at mid span of the compressed material fibres triples the critical buckling load. The reason is that the renewed boundary condition actually forces the beam into higher buckling modes, which correspond with higher eigenvalues or critical loads.

In contradiction with the constant load, both curves, which correspond to a point load, are very clearly separated and do not show any points of intersection. Moreover, the difference between the corresponding load factor values of both curves remains very well pronounced for the total range of spring stiffnesses k. Since we wanted to understand why we found such an important influence of the additional lateral support here and not in the previous loading type, we checked some additional loading types, as described below.

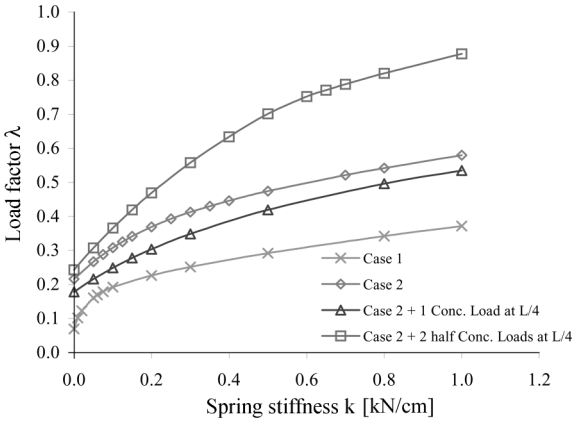

Fig. 10 Results for the concentrated load

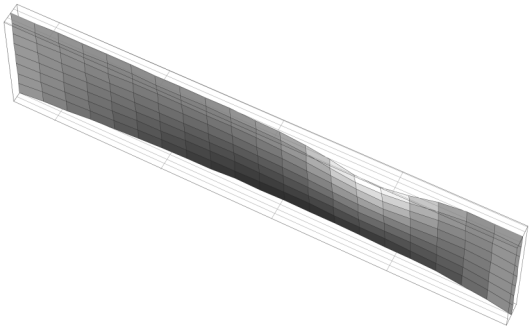

Fig. 11 Buckling mode for extra loading cases (k = 1 kN/cm)

4.5 Additional loading types

Two more loading types have been simulated (Fig. 10) in combination with the boundary condition case 2 (i.e. with one additional lateral restraint at mid span). In the first extra loading type, the point load P is positioned on a quarter length of the beam. For this position, a maximum lateral deflection is expected for the "second" eigenmode of the unrestrained beam, in which the beam is forced by the present boundary conditions. In comparison with a load position at mid span (simple Case 2) load factors lie now below that previous curve (Fig. 10).

In the second extra loading type, two local loads, each of magnitude equalling half the value of the initial load, are placed at a quarter point of the span. Spreading the load into two half loads $P/2$ gives a more favourable situation than concentrating it at one location, as we see the position of the corresponding curve of the load factor lying far above the previous one. We notice that the curve of the load factors found is lying in between the curves of one point load and a constant load over the full length (Fig. 10). Hence that all loading types represent the same total force of 132000 N!

5. Experiments

5.1 Aluminium - glass

For the first experiments, aluminium is chosen as the material for the scale models, because it is easier to produce test specimens, and costs are relatively low. The value of Young's modulus for aluminium as found in literature is 70000 MPa. For the glass used in the laboratory, the Young's modulus has been obtained from laboratory bending tests, resulting in a value of 70432 MPa. The Young's moduli of aluminium and glass are very similar, so rectangular aluminium strips initially seem to be a valid alternative to examine instability problems of glass beams (Roelandt 2000).

The results of the numerical analysis are confirmed by the experiments. However, not all cases have been experimentally tested at this moment. The research on glass specimens is in progress.

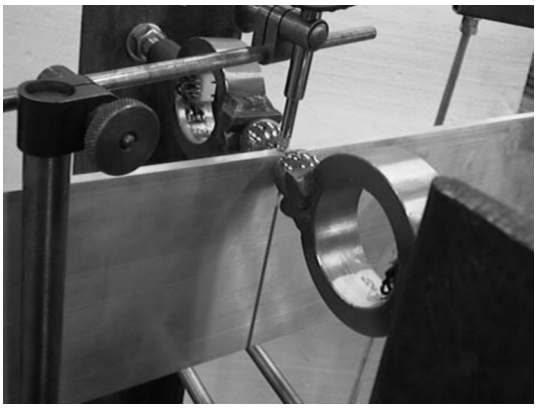

Fig. 12 Lateral restraints

5.2 Test set-up

In order to simulate the theoretical boundary conditions as good as possible, the beam is supported by steel fork bearings, which mechanically allow translations and rotations as described above. At the moment of submission of this paper, loading types are limited to point loads.

5.2.1 Small specimens

In a first stage, tests are performed on small aluminium and glass specimens with dimensions of 1000 mm length, 100 mm height and 3 mm thickness. The thickness is chosen such that the critical load for lateral torsional buckling lies relatively far below the load, which causes the in plane bending to reach a critical value.

Because of the sensitivity to small forces of the test set-up, loads are introduced in the system by placing masses of only 1 and 0.5 kg on a pendulum below the beam. The pendulum itself is hinge-connected with the beam and stays vertical during the test, independently from small lateral beam deformations. The dynamic effects of its lateral movements are diminished by a viscous fluid dampener. Lateral point-wise restraints of the compressed upper rim are realised by steel spheres, which are laterally fixed to the test set-up frame at both sides of the beam (Fig. 12). In a further stage, an elastic foundation effect is realised by means of a continuous silicon joint between the beam and a roof panel with negligible flexural out-of-plane stiffness. Dynamometers are used to control lateral reaction forces in the restraints. Displacements are measured with electronic devices, placed at the positions on the beam where maximum deflections are expected by the numerical simulations (Chapter 4). Lateral and vertical displacement measurements at these positions are combined with vertical displacement measurements at the fixed lateral supports.

The value for the critical lateral torsional buckling load, calculated for a beam with the same dimensions as the experimental aluminium models, is 323.81 N. This load corresponds to a bending stress of 16.2 MPa. Lateral torsional buckling will be the critical effect that causes collapse.

5.2.2 Larger specimens

In a second stage, tests are executed on full-scale single pane glass beams. Since the forces needed there are of the order of magnitude of plus 10 kN, loads are introduced by means of a

Fig. 13 Buckling of large specimen

hydraulic jack. A mechanical translation system permits the hydraulic jack to follow any lateral out-of-plane movement of the beam. The importance of the lateral displacements of a buckling beam is illustrated in Fig. 13. The verticality of the load remains guaranteed this way. All vertical and horizontal displacements are quantified electronically. Again, the position of the lateral and vertical displacement measurement devices is based on the numerical simulations, and extra vertical displacement measurement equipment is placed at the individual lateral restraints.

5.3 Determination of the critical load P_{cr}

The lateral out-of-plane movement δ which is typical for lateral torsional buckling, is defined as follows (Southwell 1932):

$$\delta = \alpha \cdot \frac{1}{\left(\frac{P_{cr}}{P}\right)^{n} - 1} \tag{4}$$

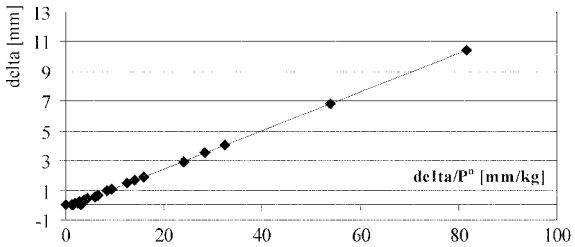

Fig. 14 Southwell diagram for aluminium test beam

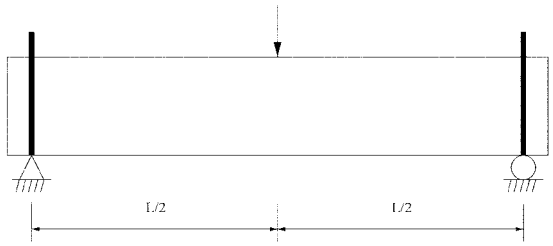

Fig. 15 Test set-up

From the experimentally obtained data for δ, it is possible to calculate the critical load P_{cr} from the relationship between δ/P^n and δ. In literature this method is known as the Southwell diagram. A typical Southwell diagram is plotted for an aluminium test beam (Fig. 14). In the case shown here, a linear relationship between δ/P^n and δ is found for $n = 1$.

5.4 Behaviour of the beam without continuous lateral elastic supports

5.4.1 Test set-up

A first series of tests deals with a set up without springs, i.e. $k = 0$ kN/cm. The applied load in case 1 ($k = 0$ kN/cm) (Fig. 15) is augmented until a significant increase in lateral displacement is measured. Several tests on aluminium are performed, of which the calculated mean value $P_{cr,\ mean}$ equals 340.87 N.

The same is done for case 2 ($k = 0$ kN/cm). The fixed point-wise support at mid span is realised with a steel sphere at both sides of the compressed upper rim of the beam (Fig. 12). Both spheres can rotate freely to avoid friction when the beam deflects in a vertical plane. Lateral displacement measuring devices were positioned at the points of largest displacement, i.e. at the quarter span points. Southwell diagram based calculations show a $P_{cr,\ mean}$ equal to 939.11 N.

5.4.2 Results for k = 0 kN/cm

The numerical buckling loads are a little bit lower than the experimental results. The ratio of failure loads corresponding with cases 1 and 2 is 2.75, whereas the numerical simulations, on the other hand, show a slightly higher ratio (Table 1). This means that there is a limited overestimation -expected on the basis of numerical results- of the positive effect of an additional point-wise lateral restraint.

Table 1 Comparison of P_{cr}

	$P_{cr,\ experimental}$ [N]	$P_{cr,\ numerical}$ [N]
Case 1	340.87	303.03
Case 2	939.11	874.46
Ratio (case 1/case 2)	2.75	2.89

5.5 Influence of the spring stiffness

5.5.1 Test set-up

The test beams are connected to a horizontal roof plate by means of a transparent silicon sealant. Generally spoken, the sealants that are used for glass connections should be selected from a list of approved structural sealants, edited by the building authorities. Since the purpose of this experiment is only to simulate a continuous elastic connection with a varying stiffness, the choice of sealant is of no importance here. Only a strip of the roof plate is applied in the experiments. The roof plate has a high flexural stiffness in its plane. Due to vertical loadings perpendicular to its plane, it shows a very flexible behaviour in order not to influence the measurements of the critical load. The way in which the sealant is applied is fairly well reproducible, so a constant thickness can be supposed. A permanent room temperature monitoring was available to keep track of the sealant's curing conditions. It was not possible to keep track of the relative laboratory air humidity. Different spring stiffnesses are obtained by testing specimens with different sealant curing times.

5.5.2 Results for $k \neq 0$ kN/cm

The numerical simulations showed that a continuous elastic lateral support of the compressed rim has a positive effect on the magnitude of the critical lateral torsional buckling load. The increase of load bearing capacity is proportionate to the spring stiffness of the continuous support. An experimental variation of the resulting spring stiffness of the joints is obtained by a variation of the sealant curing time. Curing times for the sealants in the experiments vary between zero and 100 hours.

By comparing the results from the experiments with the theoretical $P_{cr} - k$ function obtained from e.g. Fig. 17, a tool is found to translate sealant curing times to the corresponding spring stiffnesses. The best fitting curve for the relationship between curing time and critical load is shown in Fig. 16.

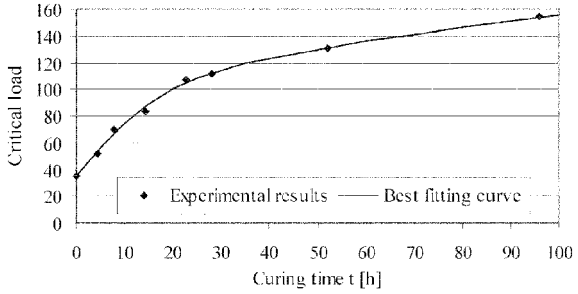

Fig. 16 Curing time towards critical load

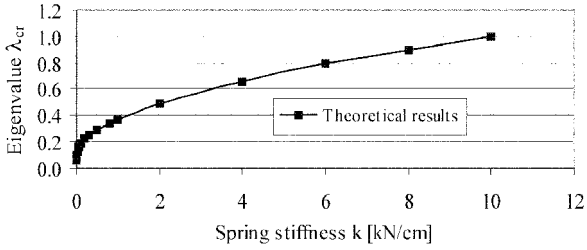

Fig. 17 Spring stiffness towards lowest eigenvalue

5.5.3 Capacity factor ψ

The capacity factor ψ is defined as the factor by which the lateral torsional buckling load bearing capacity increases when the spring stiffness k or the curing time t augment.

$$\psi = \frac{P_{cr}}{P_{cr,\,t=0}} = \frac{\lambda_{cr}}{\lambda_{cr,\,k=0}} \tag{5}$$

Fig. 17 shows that the most important increase of the eigenvalue appears in a relatively small interval of low values of k. For this interval, the $\psi - k$ and $\psi - t$ relationships are examined and plotted in Fig. 18.

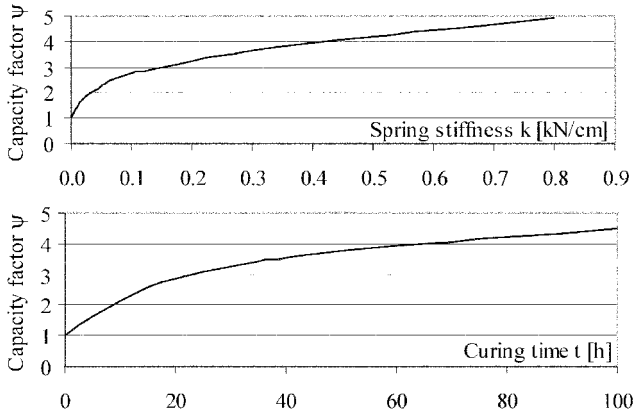

Fig. 18 Comparison of spring stiffness and curing time

Finally, we combine the findings above to establish a relationship between t and k for the applied sealant cross section (Fig. 19):

$$k = 0.0062\ t \tag{6}$$

In the limit case when the value for the curing time t grows to infinity, a finite maximum value for the spring stiffness k is expected.

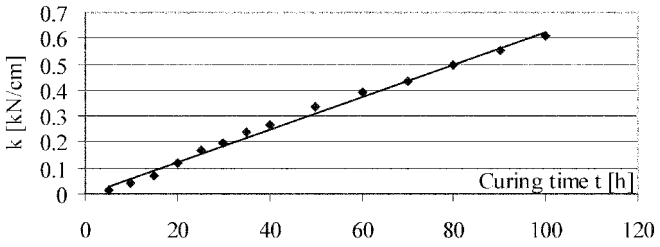

Fig. 19 Curing time against spring stiftness

6. Conclusions

Analogous conclusions could be drawn from numerical analysis and preliminary experiments:

6.1 Lateral restraints

The addition of point-wise lateral restraints has a very important positive effect on the load bearing capacity of a beam subjected to a concentrated load. For constant loads, the effect is significant only for cases with "weak" springs ($k < 0.1$ kN/cm). If the compressed rim is laterally continuously supported by stiffer springs, point-wise lateral restraints are not very useful. e.g. if glass beams are silicon-glued to the roof structure, stabilising cables could be omitted in the design.

6.2 Spring stiffness

Independently from loading type or boundary condition case, the attachment of continuous lateral springs at the compressed rim obviously increases the strength of the beam. When the eigenvalues for lateral torsional buckling are plotted against the value of the spring stiffness, it is shown that the effect of an increase of the spring stiffness is most pronounced for small values of the spring stiffness, where the rise of the eigenvalue diagram is rather steep. For larger values of the spring stiffness, rate of gain in strength gets smaller for a given value of the increase of spring stiffness.

6.3 Loading types

In comparison to a local load at mid span, the load bearing capacity of the beam is higher if the same load is uniformly spread over the length of the beam. This was expected since the maximum bending moments are doubled for local loads ($M_p = \frac{Pl}{4} = \frac{pl^2}{4}$ against $M_p = \frac{pl^2}{8}$).

6.4 Realistic sealant joints

The influence of a real sealant joint on the lateral torsional buckling behaviour of the glass beam is examined experimentally. The experimental results are coupled to the numerical results, by relating the curing time of the sealant to the numerical spring stiffness. For the examined sealant, geometry and range of spring stiffnesses, the relationship is a linear one.

7. Future research

In near future more laboratory experiments will be executed on large glass models with other geometries. Tests on laminated glass specimens will be performed.

At this moment, the value of spring constants of the lateral supporting springs is being interpreted and translated towards a wider range of realistic supports. These realistic point-wise supports could e.g. be steel cables; realistic continuous supports could be realised by transparent silicones.

A geometrical parameter study on the lateral torsional buckling load for beams with lateral supports is in progress, in order to generalise our conclusions to beams with other geometries.

References

Belis, J. (2001), "Glass beams", *Proceedings of the Second FTW PhD Symposium*, Ghent, December.

Belis, J., Van Impe, R., Lagae, G. and Buffel, P. (2001), "Glass and transparent plastics: a structural engineering point of view", *Proceedings of the 7th European Conference on Advanced Materials and Processes*, Rimini, June.

Belis, J. (2000), "Glass structures", *Proceedings of the First FTW PhD Symposium*, Ghent, December.

Calderdone, I. (2001), "The fallacy of the Weibull distribution for window glass design", *Proceedings of the Glass Processing Days*, Tampere, June.

Carré, H. (1997), Tempered Glass, A New Structural Material (in French), *Cahiers du CSTB*, Cahier 3003.

Griffith, A. (1921), "The phenomena of rupture and flow in solids", *Phil. Trans. Roy. Soc. of London*, **221**.

Hess, R. (2000), *Glass Beams* (in German), vdf Hochschulverlag AG an der ETH Zürich, Zürich.

NBN-ENV 1993-1-1, Eurocode 3 (1992), *Design of Steel Structures - Part 1-1: General Rules and Rules for Buildings*, Belgian Institute for Normalisation (BIN) vzw.

The Institute of Structural Engineers (ISE) (1999), *Structural Use of Glass in Buildings*, SETO, London.

Pattheeuws, S. (2001), "Calculation of lateral torsional buckling loads with finite elements method", Graduate thesis (in Dutch), Ghent.

Roelandt, M. (2000), "Lateral torsional buckling of glass beams", Graduate thesis (in Dutch), Ghent.

Southwell, R.V. (1932), "On the analysis of experimental observations in problems of elastic stability", *Proceedings of the Royal Society*, **135A**, London, 601.

Timoshenko, S. and Gere, J. (1991), *The Theory of Elastic Stability*, 2nd edition, McGraw-Hill Book Company Inc., New York/Toronto/London.

Trahair, N. (1993), *Flexural-Torsional Buckling of Structures*, E&FN Spon, London.

Van Impe, R. (1998), *Calculation of Constructions with Rasta*, manual v 3.0 (in Dutch).

Vernaillen, F. (2002), "Prevention of lateral torsional buckling of glass beams", Graduate thesis (in Dutch), Ghent.

Weibull, W. (1951), "A statistical distribution function of wide applicability", *J. of Appl. Mech.*, September 1951, 293-297.

Young, W. (1989), *Roark's Formulas for Stress and Strain*, 6th edition, McGraw-Hill Book company Inc., New York/Toronto/London.